

Membrane-bound O-acyltransferase 7 (MBOAT7) shapes lysosomal lipid homeostasis and function to control alcohol-associated liver injury

Venkateshwari Varadharajan^{1,2,3}, Iyappan Ramachandiran^{1,2,3}, William J Massey^{1,2,3}, Raghav Jain⁴, Rakhee Banerjee^{1,2,3}, Anthony J Horak^{1,2,3}, Megan R McMullen^{3,5}, Emily Huang^{3,5}, Annette Bellar³, Shuhui W Lorkowski⁶, Kailash Gulshan⁷, Robert N Helsley^{1,8}, Isabella James⁴, Vai Pathak^{3,5}, Jaividhya Dasarathy^{3,9}, Nicole Welch^{3,5}, Srinivasan Dasarathy^{2,3,5}, David Stroom¹⁰, Ofer Reizes², Daniela S Allende^{3,11}, Jonathan D Smith¹, Judith Simcox⁴, Laura E Nagy^{2,3,5}, J Mark Brown^{2,3*}

¹Department of Cancer Biology, Lerner Research Institute of the Cleveland Clinic, Cleveland, United States; ²Center for Microbiome and Human Health, Lerner Research Institute, Cleveland Clinic, Cleveland, United States; ³Northern Ohio Alcohol Center (NOAC), Lerner Research Institute, Cleveland Clinic, Cleveland, United States; ⁴Department of Biochemistry, University of Wisconsin-Madison, Madison, United States; ⁵Department of Inflammation and Immunity, Lerner Research Institute, Cleveland Clinic, Cleveland, United States; ⁶Department of Cardiovascular and Metabolic Sciences, Lerner Research Institute of the Cleveland Clinic, Cleveland, United States; ⁷Center for Gene Regulation in Health and Disease (GRHD), Cleveland State University, Cleveland, United States; ⁸Department of Pharmacology & Nutritional Sciences, Saha Cardiovascular Research Center, University of Kentucky College of Medicine, Lexington, United States; ⁹Department of Family Medicine, Metro Health Medical Center, Case Western Reserve University, Cleveland, United States; ¹⁰Lutheran Hospital, Cleveland Clinic, Cleveland, United States; ¹¹Department of Anatomical Pathology, Cleveland Clinic, Cleveland, United States

*For correspondence: brownm5@ccf.org

Competing interest: See page 17

Funding: See page 17

Sent for Review
11 September 2023
Preprint posted

27 September 2023

Reviewed preprint posted
27 December 2023

Reviewed preprint revised
04 March 2024

Version of Record published
22 April 2024

Reviewing Editor: Pramod K Mistry, Yale University, United States

© Copyright Varadharajan et al. This article is distributed under the terms of the [Creative Commons Attribution License](#), which permits unrestricted use and redistribution provided that the original author and source are credited.

Abstract Recent genome-wide association studies (GWAS) have identified a link between single-nucleotide polymorphisms (SNPs) near the MBOAT7 gene and advanced liver diseases. Specifically, the common MBOAT7 variant (rs641738) associated with reduced MBOAT7 expression is implicated in non-alcoholic fatty liver disease (NAFLD), alcohol-associated liver disease (ALD), and liver fibrosis. However, the precise mechanism underlying MBOAT7-driven liver disease progression remains elusive. Previously, we identified MBOAT7-driven acylation of lysophosphatidylinositol lipids as key mechanism suppressing the progression of NAFLD (Gwag et al., 2019). Here, we show that MBOAT7 loss of function promotes ALD via reorganization of lysosomal lipid homeostasis. Circulating levels of MBOAT7 metabolic products are significantly reduced in heavy drinkers compared to healthy controls. Hepatocyte- (*Mboat7*-HSKO), but not myeloid-specific (*Mboat7*-MSKO), deletion of *Mboat7* exacerbates ethanol-induced liver injury. Lipidomic profiling reveals a reorganization of the hepatic lipidome in *Mboat7*-HSKO mice, characterized by increased endosomal/lysosomal lipids. Ethanol-exposed *Mboat7*-HSKO mice exhibit dysregulated autophagic flux and lysosomal biogenesis, associated with impaired transcription factor EB-mediated lysosomal biogenesis and autophagosome accumulation. This study provides mechanistic insights into how MBOAT7 influences

ALD progression through dysregulation of lysosomal biogenesis and autophagic flux, highlighting hepatocyte-specific MBOAT7 loss as a key driver of ethanol-induced liver injury.

eLife assessment

Varadharajan et al. explore the mechanistic basis of MBOAT7 SNP association with steatotic liver disease and link its function in LPI acylation to altered lipidomics of endosomal/lysosomal system and impaired TFEB mediated lysosomal biogenesis. The findings are **important** with theoretical and practical implications in MAFLD, alcohol-induced hepatic steatosis, and lysosomal diseases. The strength of evidence is **convincing** using methodology in line with current state-of-the-art.

Introduction

End-stage liver diseases account for approximately 2 million deaths annually worldwide, with nearly half of liver disease-associated deaths arising from complications of alcohol-associated and non-alcoholic fatty liver disease (NAFLD)-related cirrhosis, and the other half driven by viral hepatitis and hepatocellular carcinoma. It is generally appreciated that there are some shared mechanisms driving liver injury from viral, NAFLD, or alcohol-associated liver disease (ALD)-driven etiologies, but also etiology-specific drivers that uniquely shape the pathogenesis of liver failure. Although there has been great progress in identifying the 'multiple hits' that lead to end-stage liver disease, we are only beginning to understand the cellular and molecular mechanisms driving etiology-specific liver disease progression. Within the evolving 'multiple hit' theory of liver disease progression, it is clear that interactions between environmental factors (i.e., diet, microbiome, alcohol, viral infection, environmental toxins, etc.) and genetic determinants uniquely contribute to liver injury (Cohen et al., 2011; Rinella and Sanyal, 2016). Currently, the only option for end-stage liver disease is liver transplantation. However, the availability of viable donor livers is finite, and pharmacological approaches to improve outcomes are simply lacking due to our poor understanding of the underlying mechanisms of disease pathogenesis. Given this, there is a clear need to understand the genetic and environmental interactions promoting the progression of liver disease from simple steatosis to more advanced inflammatory and fibrotic disease. We address this gap here by investigating the mechanisms linking a recently identified liver disease susceptibility gene in combination with alcohol exposure.

Genome-wide association studies (GWAS) provide a powerful unbiased tool to identify new genes contributing to human disease, allowing for pinpoint accuracy in identification of new potential drug targets. This is exemplified by the recent success story of GWAS discoveries leading to rapid development of monoclonal antibodies targeting proprotein convertase subtilisin/kexin type 9 (PCSK9) for hyperlipidemia and cardiovascular diseases (Sabatine, 2019). Since 2015, several independent GWAS studies have identified a liver disease susceptibility locus (rs641738) near the genes encoding MBOAT7 and TMC4 (Buch et al., 2015; Mancina et al., 2016; Krawczyk et al., 2017; Thabet et al., 2016; Thabet et al., 2017; Teo et al., 2021). It is important to note that the rs641738 T-allele (~43% allele frequency in European ancestry populations) is associated with all major forms of liver injury including NAFLD, ALD, and viral hepatitis-induced fibrosis (Buch et al., 2015; Mancina et al., 2016; Krawczyk et al., 2017; Thabet et al., 2016; Thabet et al., 2017; Teo et al., 2021). The rs641738 variant is associated with a C>T missense single-nucleotide polymorphism (SNP) within the first exon the TMC4 gene, but the GTEx project shows that TMC4 is not abundantly expressed in human liver (1.4 transcripts per million). We previously showed that mice lacking *Tmc4* (*Tmc4*^{-/-}) have normal high fat diet-induced hepatic steatosis (Gwag et al., 2019). We also recently demonstrated that anti-sense oligonucleotide (ASO)-mediated knockdown of *Mboat7* promotes insulin resistance, hepatic steatosis, hepatocyte death, inflammation, and early fibrosis in high fat diet-fed mice (Gwag et al., 2019). In parallel, four independent groups also showed that *Mboat7* loss of function promotes hepatic steatosis, inflammation, and fibrosis in mice (Meroni et al., 2020; Tanaka et al., 2021; Thangapandi et al., 2021; Xia et al., 2021). Collectively, MBOAT7 is a genetic determinant of advanced liver disease, but how this gene shapes susceptibility to environmental cues is still an area of intense investigation.

The MBOAT7 gene encodes a lysophospholipid acyltransferase enzyme (also known as lysophosphatidylinositol acyltransferase 1, LPIAT1), which uniquely contributes to the Land's cycle of

membrane phospholipid remodeling (*Shindou and Shimizu, 2009*). The Land's cycle is a series of phospholipase-driven deacylation and lysophospholipid acyltransferase-driven acylation reactions that shape membrane asymmetry and diversity (*Shindou and Shimizu, 2009*). It is important to note that MBOAT7 selectively diversifies the fatty acid composition of membrane phosphatidylinositol (PI) species and not phospholipids with other head groups and exhibits acyl chain specificity for polyunsaturated fatty acids (*Shindou and Shimizu, 2009; Gijón et al., 2008; Zarini et al., 2014*). This substrate specificity has been observed in in vitro or cell-based studies (*Gijón et al., 2008; Zarini et al., 2014*), which has been confirmed in vivo in mice with diminished *Mboat7* function (*Gwag et al., 2019; Meroni et al., 2020; Tanaka et al., 2021; Thangapandi et al., 2021; Xia et al., 2021*). Although MBOAT7 is well documented to directly modulate PI lipids, the Land's cycle is highly dynamic and has the potential to influence many downstream metabolic processes as well as cell signaling. Here, we report that ethanol-induced perturbation of the hepatic lipidome is powerfully shaped by MBOAT7 function in hepatocytes. This MBOAT7-dependent reorganization of the hepatic lipidome in response to ethanol is also functionally tied to diminished lysosome function and defective autophagy. This work shows that MBOAT7 uniquely contributes to ethanol-induced liver injury via perturbations of hepatic lipid metabolism that extend beyond the direct remodeling of membrane PI.

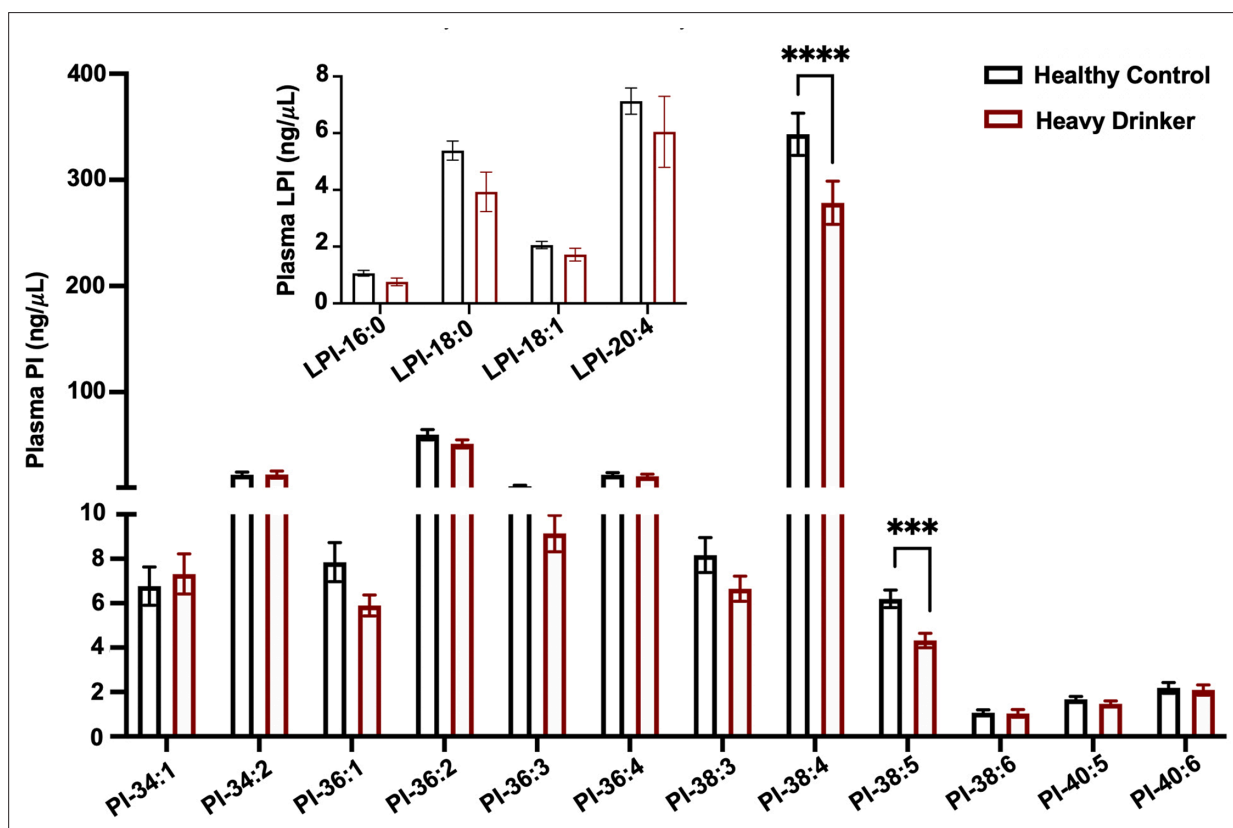


Figure 1. MBOAT7 products are selectively reduced in heavy drinkers. Plasma lysophosphatidylinositol (LPI – inset graph) and phosphatidylinositol (PI) species from both male and female healthy controls and heavy drinkers were measured by liquid chromatography–tandem mass spectrometry (LC–MS/MS). $n = 10–16$; *** $p < 0.001$ and **** $p < 0.0001$ in the figure. Analysis of variance (ANOVA) with Tukey's post hoc test.

The online version of this article includes the following source data for figure 1:

Source data 1. Demographic and clinical parameters for the entire cohort of healthy controls and heavy drinkers recruited for this study.

Results

Heavy drinkers have reduced circulating levels of MBOAT7 enzymatic products

Given previous studies have shown that MBOAT7 is a risk locus for alcohol-associated cirrhosis (Buch et al., 2015), we investigated whether active alcohol consumption was associated with alterations in MBOAT7 function. To address this, we measured both lysophosphatidylinositol (LPI) substrates and PI products of the MBOAT7 enzymatic reaction in the circulation of healthy controls compared to confirmed heavy drinkers (Figure 1). Heavy drinkers were recruited and defined by an AUDIT score (Fleming et al., 1991) greater than 16, and compared to an age- and sex-matched healthy control population (Figure 1—source data 1). In agreement with genetic studies linking MBOAT7 variants to alcohol-associated cirrhosis (Buch et al., 2015), we find that circulating levels of metabolic products of MBOAT7 including arachidonic acid- and eicosapentaenoic acid-containing phosphatidylinositols (PI 38:4 and PI 38:5) are significantly reduced in heavy drinkers compared to age-matched healthy controls (Figure 1). Given MBOAT7 demonstrates specificity for polyunsaturated (PUFA) acyl-CoA substrates (Gijón et al., 2008), it is important to note that only select PUFA-containing MBOAT7 products (PI 38:4 and PI 38:5) were reduced in heavy drinkers, whereas all other molecular species of PI were unaltered. We also examined the circulating levels LPI substrates of MBOAT7 but found no significant differences between controls and heavy drinkers (Figure 1). These data show that excessive alcoholic intake is associated with reduced levels of MBOAT7 product lipids, which further bolsters the concept that MBOAT7 loss of function may be causally linked to ALD progression.

MBOAT7 loss of function in hepatocytes, but not myeloid cells, facilitates ethanol-induced liver injury in mice

Although there is some emerging evidence that MBOAT7 genetic variants may predispose humans to alcohol-induced liver injury (Buch et al., 2015), not all human studies have found a significant association (Zhang et al., 2018; Stickel et al., 2018; Beaudoin et al., 2021). Importantly, a causal relationship between MBOAT7 and alcohol-induced liver injury has never been established to date. To address this, we have studied ethanol-induced liver injury in mice selectively lacking *Mboat7* in hepatocytes or myeloid cells, given the key roles that hepatocytes and myeloid cells play in the pathogenesis of ethanol-induced liver disease progression. To generate congenic hepatocyte-specific (*Mboat7*-HSKO) and myeloid-specific (*Mboat7*-MSKO) *Mboat7* knockout mice we crossed mice harboring a post-FLP recombinase conditionally targeted *Mboat7* floxed allele (Anderson et al., 2013; Massey et al., 2023) to mice transgenically expressing Cre recombinase under the albumin promoter/enhancer (Postic et al., 1999) or Cre knocked into the M lysozyme locus (Clausen et al., 1999), respectively. These independent *Mboat7*-HSKO and *Mboat7*-MSKO lines were then backcrossed mice >10 generations into the C57BL/6J background and subsequently subjected to ethanol exposure. Compared to control mice (*Mboat7*^{fllox/fllox}), *Mboat7*-HSKO mice had significantly reduced *Mboat7* mRNA and protein expression in the liver (Figure 2A, B), but not in other tissues (data not shown; Massey et al., 2023). Hepatocyte-specific deletion of *Mboat7* resulted in enhanced ethanol-induced increases in liver weight and high concentrations of plasma alanine aminotransferase (ALT) (Figure 2C, D). Likewise, *Mboat7*-HSKO mice showed elevated hepatic steatosis scores and triglyceride levels under both pair-fed and ethanol-fed conditions (Figure 2E, F). However, hepatocyte-specific deletion of *Mboat7* did not significantly alter the mRNA expression for several proinflammatory cytokines/chemokines including tumor necrosis factor α (*Tnfa*), transforming growth factor β (*Tgfb*), monocyte chemoattractant protein 1 (*Mcp1*), or interleukins 1 β (*Il1b*) or 6 (*Il6*) in either pair- or ethanol-fed conditions (Figure 2G). These data demonstrate that MBOAT7 function in hepatocytes is a critical determinant of ethanol-induced liver injury, but we also wanted to explore a potential role for MBOAT7 in non-parenchymal cells given the key roles that macrophages and neutrophils play in ALD.

It is important to note during the preparation of this manuscript, an independent study discovered a potential role for MBOAT7 in suppressing toll-like receptor signaling and proinflammatory cytokine production in macrophages and Kupffer cells in the context of NAFLD (Alharthi et al., 2022). Furthermore, early studies examining the expression and substrate specificity for diverse lysophospholipid acyltransferases showed that MBOAT7-driven PI remodeling was highly active in human neutrophils where it can modulate the production of proinflammatory arachidonic acid-derived lipid mediators

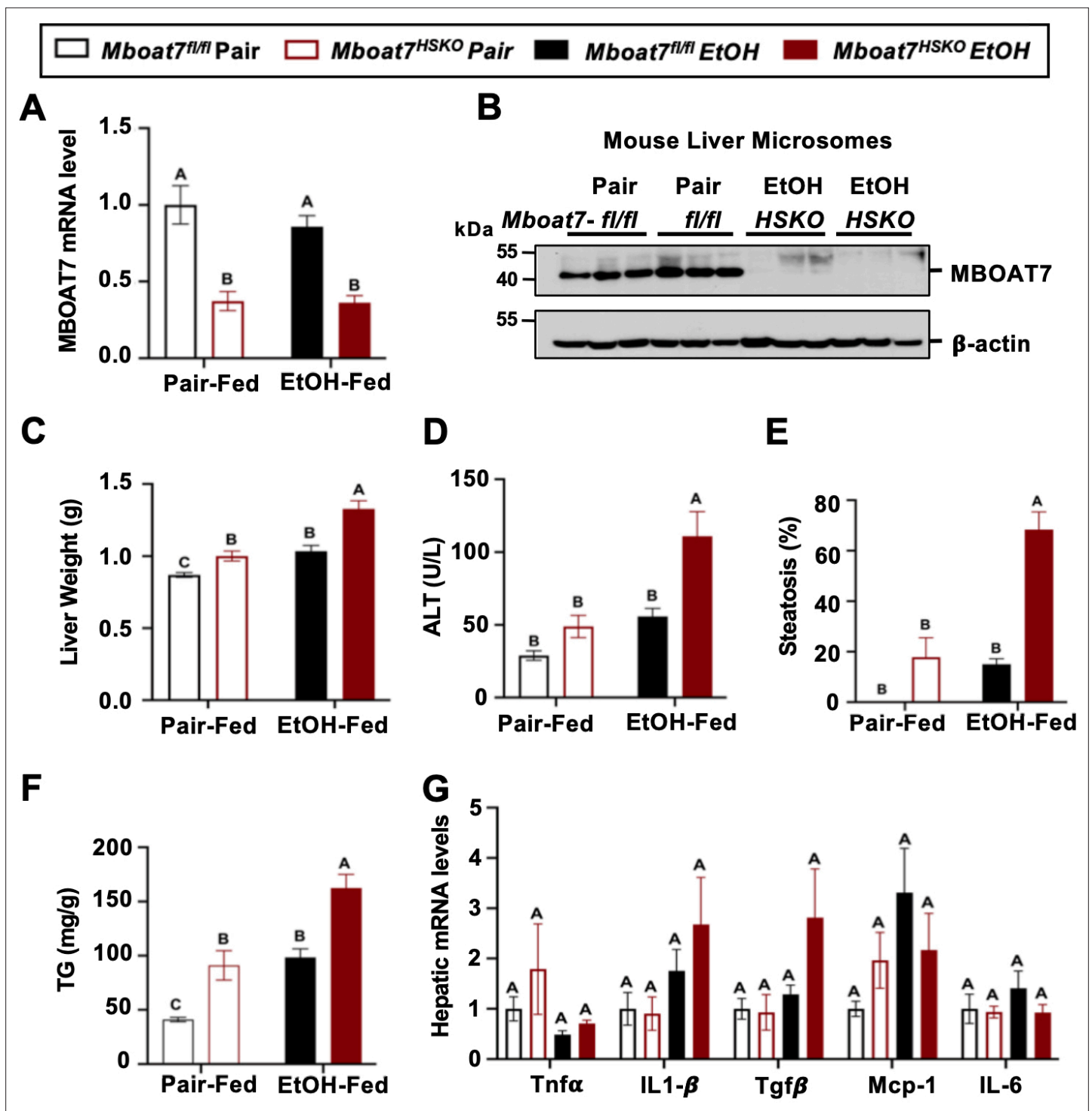


Figure 2. Hepatocyte-specific deletion of *Mboat7* promotes ethanol-induced liver injury. Female control (*Mboat7^{fl/fl}*) or hepatocyte-specific *Mboat7* knockout mice (*Mboat7*-HSKO) were fed with subjected the NIAAA (National Institute on Alcohol Abuse and Alcoholism) model of ethanol-induced liver injury. (A) Hepatic *Mboat7* expression was measured via quantitative polymerase chain reaction (qPCR). (B) Western blot for hepatic microsomal MBOAT7 protein levels replicated in $n = 3$ mice. (C) Liver weight, (D) plasma alanine aminotransferase (ALT), (E) percent steatosis quantified by a blinded board-certified pathologist, (F) hepatic triglycerides, and (G) hepatic expression of inflammatory gene measured by qPCR. $n = 5-7$. Data represent the mean \pm standard error of the mean (SEM) and groups not sharing a common letter superscript differ significantly ($p \leq 0.05$).

The online version of this article includes the following source data and figure supplement(s) for figure 2:

Source data 1. Original file for the western blot analysis in **Figure 2B** (anti-MBOAT7 and anti- β -actin).

Figure 2 continued on next page

Figure 2 continued

Source data 2. PDF containing **Figure 2B** and original scans of the relevant western blot analysis (anti-MBOAT7 and anti- β -actin) with highlighted bands and sample labels.

Figure supplement 1. Myeloid-specific deletion of *Mboat7* does not promote ethanol-induced liver injury.

Figure supplement 1—source data 1. Original file for the western blot analysis in **Figure 2A** (anti-MBOAT7 and anti- β -actin).

Figure supplement 1—source data 2. PDF containing **Figure 2A** and original scans of the relevant western blot analysis (anti-MBOAT7 and anti- β -actin) with highlighted bands and sample labels.

(Gijón *et al.*, 2008). Therefore, we generated myeloid-specific (*Mboat7*-MSKO) *Mboat7* knockout mice to further interrogate cell autonomous roles in ALD progression. First to confirm efficient deletion in myeloid cells, we isolated both bone marrow-derived and thioglycolate-elicited macrophages from control and myeloid-specific (*Mboat7*-MSKO) *Mboat7* knockout mice, which confirmed essentially no detectable MBOAT7 protein in *Mboat7*-MSKO mice (**Figure 2—figure supplement 1**). In contrast to the enhanced ethanol-induced liver injury seen in *Mboat7*-HSKO mice (**Figure 2**), myeloid-specific (*Mboat7*-MSKO) *Mboat7* deletion resulted in unaltered ethanol-induced effects on body weight, liver weight, circulating levels of aspartate and alanine aminotransferases (AST and ALT), liver triglyceride, and cytokine expression (**Figure 2—figure supplement 1**). Collectively, these results demonstrate that MBOAT7 loss of function in hepatocytes, but not myeloid cells, facilitates ethanol-induced liver injury in mice.

Ethanol exposure reorganizes the hepatic lipidome in a MBOAT7-dependent manner

Given the fact that ethanol exposure is well known to reorganize hepatic lipid metabolism, we performed comprehensive lipidomic profiling of the liver to understand how MBOAT7 could potentially shape ethanol-induced lipid metabolism in the liver. First, we used a targeted approach to measure the levels of MBOAT7 substrate LPIs and product PIs. Compared to control mice (*Mboat7*^{fl^{ox}/fl^{ox}}), *Mboat7*-HSKO mice had significant accumulation of palmitate- and oleate-containing LPI substrate lipids (LPI 16:0 and LPI 18:1), with large accumulation of LPI 16:0 under ethanol-fed conditions (**Figure 3A**). When we examined PI species, we confirmed previous findings that *Mboat7*-HSKO mice have reduced levels of the major arachidonic acid-containing PI (PI 38:4) and also striking reductions in PI 38:3 under both pair- and ethanol-fed conditions (**Figure 3B**). In addition, *Mboat7*-HSKO mice also have accumulation of several other PI species including PI 34:1, PI 36:1, PI 36:2, PI 38:6, and PI 40:6, some of which are exacerbated in the ethanol-fed group (**Figure 3C**). Although many of these changes in MBOAT7's substrate LPIs and product PIs are expected based on MBOAT7's substrate specificity and previous literature, there is a clear interaction between ethanol and MBOAT7 uncovered here that has not been observed in studies using NAFLD-related models (Tanaka *et al.*, 2021; Thangapandi *et al.*, 2021; Xia *et al.*, 2021).

Given this unexpected interaction between ethanol exposure and MBOAT7 within the inositol-containing phospholipid pool, we examined the hepatic lipidome more broadly. Using untargeted lipidomics, we identified a striking remodeling of the global hepatic lipidome upon ethanol feeding in *Mboat7*-HSKO mice (**Figure 3; Figure 3—figure supplements 1–11**). Unexpectedly, we observed a large increase in the levels of endosomal/lysosomal lipids including bis(monoacylglycero)phosphates (BMPs) and their outer mitochondrial membrane precursor phosphatidylglycerols (PGs) in ethanol-exposed *Mboat7*-HSKO mice (**Figure 3E–G; Figure 3—figure supplements 3 and 4**). In addition, *Mboat7*-HSKO mice had elevated levels of cardiolipin species, which are known to localize to mitochondria (**Figure 3E and H; Figure 3—figure supplement 5**). Under the pair- and ethanol-fed conditions studies here, *Mboat7*-HSKO mice also exhibited some more minor alterations in certain species of phosphatidylcholine (PC), phosphatidylethanolamine (PE), phosphatidylserine (PS), phosphatidic acid (PA), sphingomyelin (SM), ceramides (Cer), and ether-linked phospholipids (**Figure 3E; Figure 3, Figure 3—figure supplements 2; 7–11**). Although several recent studies examining hepatocyte-specific *Mboat7*-HSKO mice have found more limited effects on the global lipidome under experimental conditions designed to stimulate non-alcoholic steatohepatitis (Tanaka *et al.*, 2021; Thangapandi *et al.*, 2021; Xia *et al.*, 2021), here we show that upon ethanol exposure, hepatocyte MBOAT7 plays a major role in shaping endosomal/lysosomal lipid homeostasis.

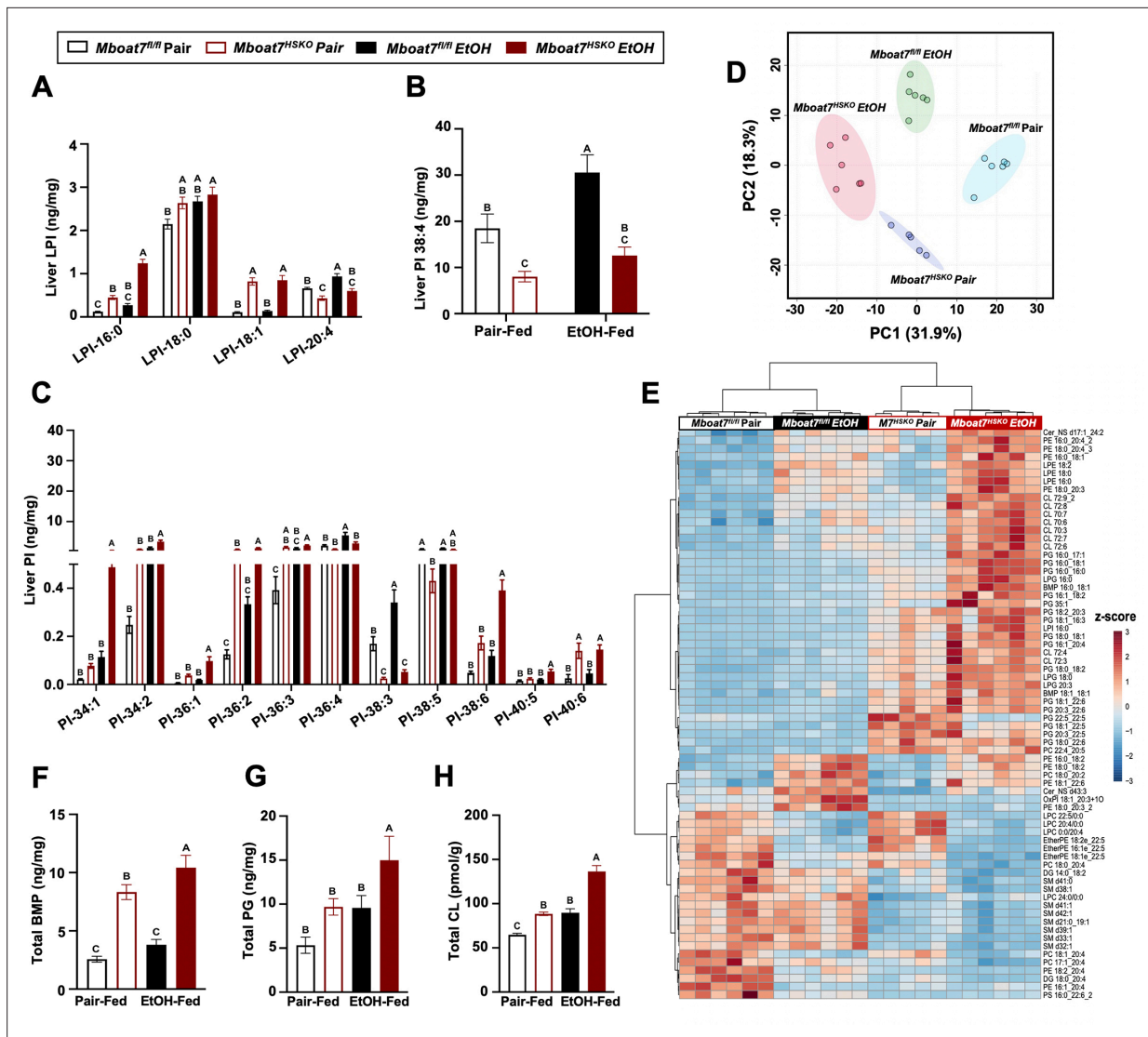


Figure 3. Ethanol alters the liver lipidome in a MBOAT7-dependent manner. *Mboat7*^{fl/fl} or *Mboat7*-HSKO mice were subjected to the NIAAA model of ethanol exposure. Liver lysophosphatidylinositol (LPI) (A) and phosphatidylinositol (PI) species, including the MBOAT7 product PI 38:4 (B) and others (C), were quantified via liquid chromatography–tandem mass spectrometry (LC–MS/MS) in *n* = 5–7. (D) Principal component analysis for untargeted lipidomics analysis. The first and second principal components are plotted on the x- and y-axis, respectively, and sample treatment group is indicated by color. (E) Heatmap showing global lipidomic alterations in mouse liver. Total levels of endosomal/lysosomal lipids were measured by targeted and untargeted lipidomic approach using LC–MS/MS. (F) Total bis(monoacylglycerol)phosphate (BMP) levels. (G) Total phosphatidylglycerol (PG) and (H) total cardiolipin (CL) from the liver of *Mboat7*^{fl/fl} or *Mboat7*-HSKO mice. Data represent the mean ± standard error of the mean (SEM) and groups not sharing a common letter superscript differ significantly (*p* ≤ 0.05).

The online version of this article includes the following figure supplement(s) for figure 3:

- Figure supplement 1.** Alterations in total hepatic lipid levels in *Mboat7*-HSKO mice.
- Figure supplement 2.** Hepatic phosphatidylcholine (PC) levels in *Mboat7*-HSKO mice.
- Figure supplement 3.** Hepatic bis(monoacylglycerol)phosphate (BMP) levels in *Mboat7*-HSKO mice.
- Figure supplement 4.** Hepatic phosphatidylglycerol (PG) levels in *Mboat7*-HSKO mice.
- Figure supplement 5.** Hepatic cardiolipin (CL) levels in *Mboat7*-HSKO mice.
- Figure supplement 6.** Hepatic phosphatidylserine (PS) levels in *Mboat7*-HSKO mice.
- Figure supplement 7.** Hepatic phosphatidylethanolamine (PE) levels in *Mboat7*-HSKO mice.
- Figure supplement 8.** Hepatic phosphatidic acid (PA) levels in *Mboat7*-HSKO mice.
- Figure supplement 9.** Hepatic sphingomyelin (SM) levels in *Mboat7*-HSKO mice.

Figure 3 continued on next page

Figure 3 continued

Figure supplement 10. Hepatic ceramide (Cer) levels in *Mboat7*-HSKO mice.

Figure supplement 11. Hepatic ether-linked lipids levels in *Mboat7*-HSKO mice.

***Mboat7*-HSKO mice have dysregulated lysosomal function in response to ethanol**

Given the accumulation of endosomal/lysosomal lipids including BMPs seen in ethanol-fed *Mboat7*-HSKO mice, we hypothesized that ethanol may perturb lysosome function in a MBOAT7-driven manner to promote liver injury. It is well known that BMPs commonly accumulate in both drug-induced and genetic lysosomal storage disorders (Gruenberg, 2020; Showalter et al., 2020; Hullin-Matsuda et al., 2014), and due to their cone-shaped structure BMPs can contribute to significant membrane asymmetry that impacts intracellular lipid sorting, apoptosis, and autophagic flux (Gruenberg, 2020; Showalter et al., 2020; Hullin-Matsuda et al., 2014). At the same time, there is emerging evidence that chronic ethanol exposure can reduce the expression of transcription factor EB (TFEB), which is a master regulator of lysosomal biogenesis and autophagy-associated gene expression (Chao et al., 2018). Given the role that lysosomal dysfunction plays in ethanol-induced liver injury (Chao et al., 2018; Bala and Szabo, 2018), and the unexpected accumulation of BMP lipids in *Mboat7*-HSKO mice, we next investigated TFEB-mediated lysosomal biogenesis and autophagy regulation in *Mboat7*-HSKO mice challenged with ethanol (Figure 4). First, *Mboat7*-HSKO mice showed elevated levels of key autophagy regulatory proteins LC3-I/II and p62 in the liver, particularly under ethanol-fed conditions (Figure 4A). Interestingly, *Mboat7*-HSKO mice also had increased total levels of the mammalian target of rapamycin (mTOR) (Figure 4A), which is a well-known master regulator of autophagic flux. The accumulation of p62 and LC3-I/II cannot distinguish between enhanced or defective autophagic flux, so we next examined potential alterations in lysosome abundance and function. Interestingly, both mRNA and protein levels of lysosomal marker proteins LAMP-1 and LAMP-2 were reduced in ethanol-fed *Mboat7*-HSKO mice (Figure 4A, D). Furthermore, compared to control mice fed ethanol, we found that ethanol *Mboat7*-HSKO mice had generally reduced expressions levels of TFEB target genes and proteins associated with lysosome acidification and lipid turnover including ATPase H⁺ transporting V1 subunits A, H, and D (*Atp6v1a*, *Atp6v1h*, and *Atp6v1d*), α galactosidase A (*Gla*), chloride channel 7 α (*Clcn7*), and mucolipin TRP cation channel 1 (*Mcoln1*) (Figure 4A, D). Similarly, the mRNA expression, and total and nuclear protein abundance of TFEB was reduced in ethanol-fed *Mboat7*-HSKO mice compared to ethanol-fed *Mboat7*^{flox/flox} control mice (Figure 4A, B and D). In contrast, the expression of key autophagy related genes including *Atg2b*, *Atg3*, *Atg7*, *Atg8*, and Unc-51-like autophagy activating kinase 1 (*Ulk1*) were significantly elevated in ethanol-fed *Mboat7*-HSKO mice compared to ethanol-fed *Mboat7*^{flox/flox} control mice (Figure 4D).

We next investigated the cell autonomous effects of ethanol on wild-type human Huh7 hepatoma cells or Huh7 cells genetically lacking MBOAT7 (Huh7- Δ MBOAT7). In agreement with what we found in mouse liver, MBOAT7 Δ -Huh7 cells had reduced levels of total TFEB and lysosomal marker proteins including LAMP1-, LAMP-2, and ATP6V1A (Figure 4—figure supplement 1). Furthermore, MBOAT7 Δ -Huh7 cells had increased levels of LC3 and total mTOR, which was particularly apparent upon ethanol exposure (Figure 4—figure supplement 1). We next assessed lysosome protein degradation activity in wild-type and MBOAT7 Δ -Huh7 hepatoma cells by measuring the degradation of an exogenous lysosome indicator, quantified via median Bodipy/Alexa647 fluorescence ratio. In the absence of ethanol treatment, there was no significant difference in the lysosomal activity between wild-type and MBOAT7 Δ -Huh7 cells. Lysosome activity was increased by 42% in wild-type cells with ethanol treatment vs. no treatment ($p < 0.001$, Figure 4C), in agreement with increased mRNA levels of several lysosomal hydrolases (Figure 4D). However, the lysosome activity was decreased by 45% in MBOAT7 Δ -Huh7 vs. wild-type cells treated with ethanol ($p < 0.001$, Figure 4C). Collectively, in the presence of EtOH, deletion of MBOAT7 in mouse or human hepatocytes results in defective TFEB-mediated lysosomal biogenesis and lysosome activity, which would be expected to lead to impaired autophagic flux.

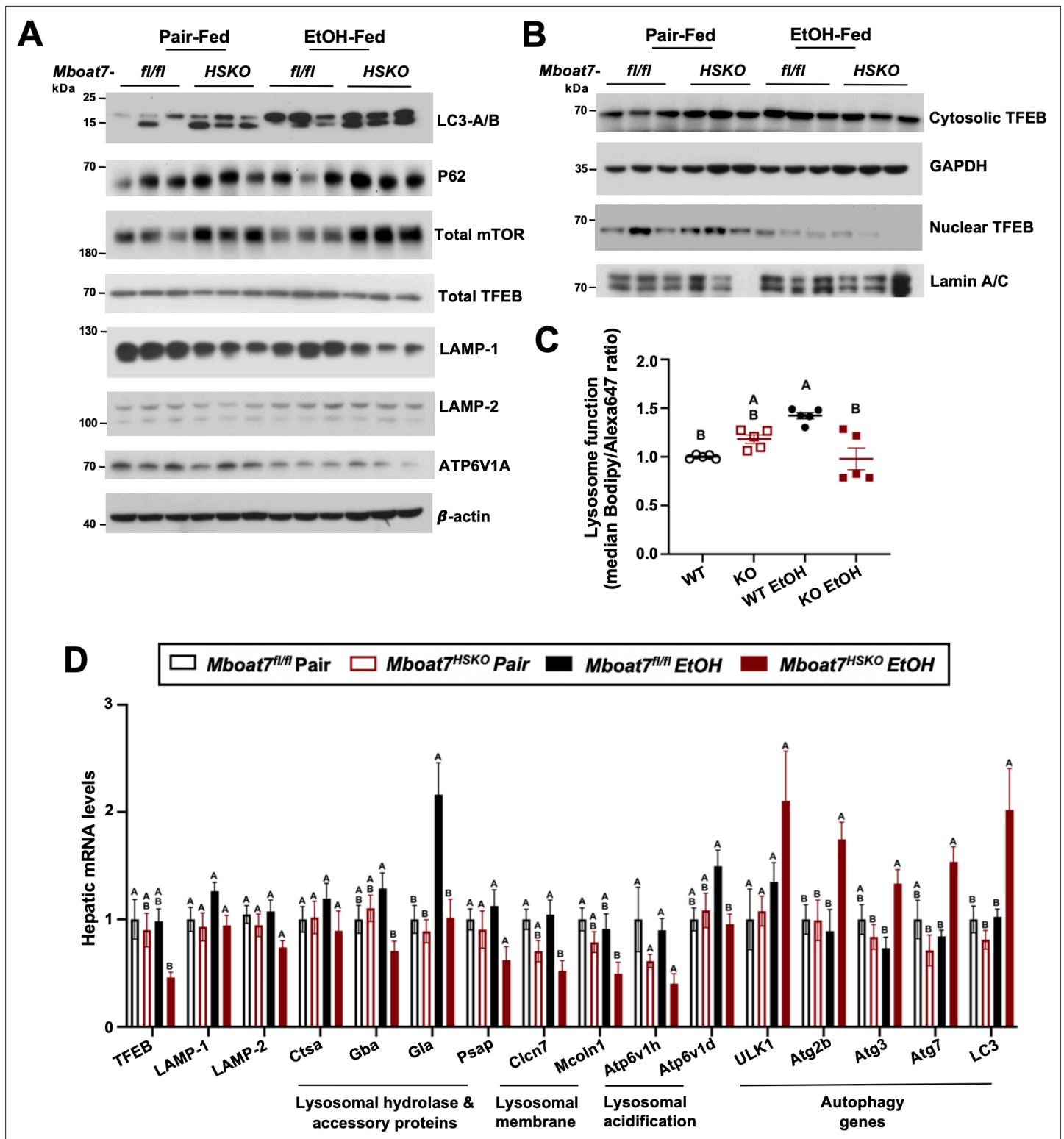


Figure 4. *Mboat7*-HSKO mice have dysregulated lysosome function in response to ethanol. Age-matched female *Mboat7*^{fl/fl} or *Mboat7*-HSKO mice were subjected to the NIAAA model of ethanol exposure. (A) Total liver lysates were subjected to western blot analysis of major autophagy marker genes LC3A/B (P62), mammalian target of rapamycin (mTOR) and lysosome biogenesis genes (TFEB, LAMP-1, LAMP-2, and ATP6V1A). (B) Nuclear fractions from mouse livers of *Mboat7*^{fl/fl} and *Mboat7*-HSKO were subjected to western blot analysis of TFEB. (C) Lysosome protein degradation activity in wild-type and MBOAT7 Δ -Huh7 hepatoma cells treated with or without 100 mM ethanol for 48 hr was assessed by incubating cells with 10 μ g/ml of lysosome indicator for 2 hr and examined by flow cytometry. *n* = 5 from two experiments by normalizing to wild-type group in each experiment; mean \pm SD. *Figure 4 continued on next page*

Figure 4 continued

standard deviation (SD) (D) Expression levels of the genes encoding functions in lysosomal hydrolase and accessory, lysosomal m involved in lysosomal biogenesis in the liver of *Mboat7^{fl/fl}* and *Mboat7-HSKO* mice upon ethanol feeding. mRNA expression levels were determined by qPCR ($n = 6/\text{group}$). Groups not sharing a common letter superscript differ significantly ($p \leq 0.05$).

The online version of this article includes the following source data and figure supplement(s) for figure 4:

Source data 1. Original file for the western blot analysis in **Figure 4A** (anti-LC3-A/B).

Source data 2. Original file for the western blot analysis in **Figure 4A** (anti-p62).

Source data 3. Original file for the western blot analysis in **Figure 4A** (anti-Total mTOR and anti-LAMP-1).

Source data 4. Original file for the western blot analysis in **Figure 4A** (anti-TFEB).

Source data 5. Original file for the western blot analysis in **Figure 4A** (anti-LAMP-2 and anti-ATP6V1A).

Source data 6. Original file for the western blot analysis in **Figure 4A** (anti- β -actin).

Source data 7. PDF containing **Figure 4A** and original scans of the relevant western blot analysis (anti-MBOAT7, anti-p62, anti-total mTOR, anti-total TFEB, anti-LAMP-1, anti-LAMP-2, anti-ATP6V1A, and anti- β -actin) with highlighted bands and sample labels.

Source data 8. Original file for the western blot analysis in **Figure 4B** (anti-cytosolic-TFEB).

Source data 9. Original file for the western blot analysis in **Figure 4B** (anti-nuclear TFEB).

Source data 10. Original file for the western blot analysis in **Figure 4B** (anti-LAMIN A/C).

Source data 11. Original file for the western blot analysis in **Figure 4B** (anti-GAPDH).

Source data 12. PDF containing **Figure 4B** and original scans of the relevant western blot analysis (anti-cytosolic TFEB, anti-nuclear TFEB, anti-LAMIN A/C, and anti-GAPDH) with highlighted bands and sample labels.

Figure supplement 1. Genetic deletion of MBOAT7 in human Huh7 cells is associated with diminished lysosome biogenesis and ethanol-induced autophagy dysregulation.

Figure supplement 1—source data 1. Original file for the western blot analysis in **Figure 4A, B** (anti-LC3-A/B).

Figure supplement 1—source data 2. Original file for the western blot analysis in **Figure 4A and B** (anti-p62).

Figure supplement 1—source data 3. Original file for the western blot analysis in **Figure 4A and B** (anti-Total mTOR and anti-LAMP-1).

Figure supplement 1—source data 4. Original file for the western blot analysis in **Figure 4A and B** (anti-TFEB).

Figure supplement 1—source data 5. Original file for the western blot analysis in **Figure 4A and B** (anti-LAMP-2 and anti-ATP6V1A).

Figure supplement 1—source data 6. Original file for the western blot analysis in **Figure 4A and B** (anti- β -actin).

Figure supplement 1—source data 7. PDF containing **Figure 4A and B** and original scans of the relevant western blot analysis (anti-MBOAT7, anti-p62, anti-total mTOR, anti-total TFEB, anti-LAMP-1, anti-LAMP-2, anti-ATP6V1A, and anti- β -actin) with highlighted bands and sample labels.

Figure supplement 2. Working model.

Discussion

This manuscript builds on our initial observation that ASO-mediated knockdown of *Mboat7* promotes NAFLD progression, hyperinsulinemia, and insulin resistance in mice (Gwag et al., 2019). Here, we have further clarified the cell autonomous roles of *Mboat7* in ethanol-driven liver injury by comparing metabolic phenotypes in hepatocyte-specific (*Mboat7-HSKO*) and myeloid-specific (*Mboat7-MSKO*) mice. The major findings of the current study include the following: (1) MBOAT7 product PI species (PI 38:4 and PI 38:5) are reduced in the circulation of human consuming high levels of alcohol; (2) MBOAT7 loss of function in hepatocytes, but not myeloid cells, promotes ethanol-induced liver injury in mice; (3) hepatocyte-specific deletion of *Mboat7* results in expected alterations in substrate LPI and product PI lipids, but unexpectedly alters lysosomal/endosome BMP lipids in an ethanol-driven manner; (4) genetic deletion in mouse or human hepatocytes results in dysregulation of lysosomal biogenesis and autophagic flux, particularly under ethanol-challenged conditions. This work provides new insights into how genetic variation in *MBOAT7* may impact ALD progression in humans and mice. Importantly, this work is the first to causally link MBOAT7 loss of function in hepatocytes, but not myeloid cells, to ethanol-induced liver injury via dysregulation of lysosomal biogenesis and autophagic flux. Although not all human studies agree there is a uniform association between the rs641738 SNP with ALD, our work indicates a very powerful interaction between MBOAT7 loss of function and ethanol-induced liver injury.

Here, we have identified a striking reorganization of the hepatic lipidome in *Mboat7-HSKO* mice when exposed to ethanol (**Figure 3; Figure 3—figure supplements 1–11**). In previous independent

studies examining lipid alterations in *Mboat7*-HSKO mice under experimental conditions to elicit NAFLD and fibrosis (i.e., high fat diets or methionine/choline-deficient diets), the global lipidomic alterations in the liver were much more confined to inositol-containing phospholipids and triacylglycerols (Tanaka et al., 2021; Thangapandi et al., 2021). It is important to note that the work of Xia and colleagues did previously report increased levels on PG lipids specifically in isolated endoplasmic reticulum (ER) membranes from *Mboat7*-HSKO mice, but our work confirms and extends this to show that not only PG but precursor BMPs are significantly elevated in *Mboat7*-HSKO mice, particularly when challenged with ethanol. It is still unclear how MBOAT7 impacts endosomal/lysosomal BMP and mitochondrial lipids such as PG and CL under ethanol-exposed conditions, but our work clearly indicates that ethanol reorganizes the global liver lipidome in a MBOAT7-dependent manner. It is most likely that the accumulation of BMP and PG lipids seen in ethanol-challenged *Mboat7*-HSKO mice are not directly related to the lysophospholipid acyltransferase activity of MBOAT7. Instead, it is more plausible that the accumulation of BMPs and PGs seen in *Mboat7*-HSKO mice is secondary to indirect reorganization of the arachidonate PI cycle or other related lipid metabolic pathways coordinated at the ER.

For instance, the arachidonate PI cycle is initiated in the ER where inositol is added to (cytidine diphosphate)CDP-diacylglycerol (18:0/20:4) by phosphatidylinositol synthase (PIS) to produce the exact same metabolic product of MBOAT7 (PI 38:4). It is likely that both PIS-generated as well as MBOAT7-generated PI 38:4 can serve as a substrate for PI kinases to form the key second messengers known as PI phosphates [PIPs including PI(18:0/20:4)-4P, PI(18:0/20:4)-4,5_{P2}] and related lipid mediators downstream of phospholipase C in the arachidonate PI cycle IP3, DAG(18:0/20:4), PA(18:0/20:4), and CDP-DAG(18:0/20:4). It is important to note that seminal work by Anderson et al., 2013 found that total PIPs, PI(18:0/20:4)-4P, and PI(18:0/20:4)-4,5_{P2} were significantly reduced in global *Mboat7*^{-/-} mice. In fact, more than 85% of PIP species in cultured cells have an *sn*-1 18:0 and *sn*-2 20:4 acyl chain composition (i.e., in part originate from the MBOAT7 and PIS product PI 38:4) (Clark et al., 2011; Rouzer et al., 2007). These reductions in PIPs seen with *Mboat7* deficiency (Anderson et al., 2013) could have important consequences in cellular signal transduction, given that PIPs are common second messengers generated downstream of ligand activation of numerous receptor systems including hormone, growth factor, cytokine, and chemokine receptors (Wymann and Schneider, 2008; Pemberton et al., 2020; Fruman et al., 2017; Hoxhaj and Manning, 2020). PIPs also play diverse roles in shaping protein–lipid interactions, membrane fusion events, vesicular transport, solute channel function, and cytoskeletal arrangement (Wymann and Schneider, 2008; Pemberton et al., 2020; Fruman et al., 2017; Hoxhaj and Manning, 2020). Most relevant to this work, anionic lipids play very important roles in controlling membrane dynamics that shape nearly all steps of autophagy including initiation of autophagosome biogenesis and autophagosome–lysosome fusion (Baba and Balla, 2020; Schink et al., 2016). Collectively, given the fact that MBOAT7 generates the most abundant species of PI (PI 38:4), and key cellular PIPs [PI(18:0/20:4)-4P and PI(18:0/20:4)-4,5_{P2}], there is a strong potential that the primary alterations in PI and PIP lipids could broadly alter cellular signal transduction, endosomal/lysosomal lipid sorting, membrane fusion events, vesicular transport, solute channel function, cytoskeletal arrangement, and autophagic flux.

Collectively, this work provides new cellular and molecular insights into how genetic variation in MBOAT7 impacts ALD progression in humans and mice. This work is the first to causally link MBOAT7 loss of function in hepatocytes, but not myeloid cells, to ethanol-induced liver injury via dysregulation of lysosomal biogenesis and autophagic flux and broaden our understanding of the lipid metabolic mechanisms promoting ethanol-induced liver injury. This work also shows that MBOAT7-driven LPI acylation in the ER can indirectly impact both lysosomal (BMP) and mitochondrial (CL and PG) lipids which can have broad impacts on autophagy described here, as well as defective fatty acid oxidation as we originally reported in high fat diet-fed mice (Gwag et al., 2019). The results of this work have broad potential implications in the management of both alcoholic- and non-alcoholic fatty liver disease, indicating that strategies that effectively restore both lysosomal and mitochondrial function may hold some therapeutic promise in humans with the common MBOAT7 rs641738 variant.

Materials and methods

Key resources table

Reagent type (species) or resource	Designation	Source or reference	Identifiers	Additional information
Genetic reagent (<i>M. musculus</i>)	<i>Mboat7tm1a(KOMP)Wtsi/Mboat7tm1a(KOMP)Wtsi</i>	PMID:23472195	RRID: MGI:5510874	
Genetic reagent (<i>M. musculus</i>)	<i>B6N.Cg-Speer6-ps1^{Tg(Alb-cre)21Mgn/J}</i>	Jackson Laboratory	Stock#: 018961 RRID: IMSR_JAX:018961	
Genetic reagent (<i>M. musculus</i>)	<i>B6.129P2-Lyz2^{tm1(cre)lfo/J}</i>	Jackson Laboratory	Stock#: 004781 RRID: IMSR_JAX:004781	
Cell line (<i>Homo sapiens</i>)	HUH7 (well differentiated human hepatocellular carcinoma)	Japanese Collection of Research Biosources Cell Bank	JCRB0403	
Antibody	Anti-MBOAT7 (Rat monoclonal)	PMID:23097495	RRID: AB_2813851	WB (1:1000)
Antibody	Anti-rat IgG HRP secondary antibody	Cell Signaling	Cat#: 7077 RRID: AB_10694715	WB (1:5000)
Antibody	LC3A/B (D3U4C) XP (Rabbit monoclonal)	Cell Signaling	Cat#: 12741 RRID: AB_2617131	WB (1:1000)
Antibody	SQSTM1/p62 (Rabbit polyclonal)	Cell Signaling	Cat#: 5114 RRID: AB_10624872	WB (1:1000)
Antibody	mTOR (7C10) (Rabbit monoclonal)	Cell Signaling	Cat#: 2983 RRID: AB_2105622	WB (1:1000)
Antibody	TFEB (D2O7D) (Rabbit monoclonal)	Cell Signaling	Cat#: 37785	WB (1:1000)
Antibody	TFEB (Rabbit polyclonal)	Thermo Fisher Scientific	Cat#: A303-673A RRID: AB_11204751	WB (1:1000)
Antibody	LAMP1 (D2D11) XP Rabbit monoclonal	Cell Signaling	Cat#: 9091 RRID: AB_2687579	WB (1:1000)
Antibody	LAMP-1 (Rat monoclonal)	Developmental Studies Hybridoma Bank (DSHB)	Cat#: ID4B RRID: AB_528127	WB (1:1000)
Antibody	LAMP-2 (Rat monoclonal)	Developmental Studies Hybridoma Bank (DSHB)	Cat#: ABL-93 RRID: AB_2134767	WB (1:1000)
Antibody	LAMP2 (D5C2P) (Rabbit monoclonal)	Cell Signaling	Cat#: 49067 RRID: AB_2799349	WB (1:1000)
Antibody	ATP6V1A (Rabbit polyclonal)	GeneTex	Cat#: GTX110815 RRID: AB_1949704	WB (1:1000)
antibody	Anti-GAPDH-HRP (Rabbit monoclonal)	Cell Signaling	Cat#: 8884 RRID: AB_11129865	WB (1:5000)
Antibody	Lamin A/C (4C11) (Mouse monoclonal)	Cell Signaling	Cat#: 4777	WB (1:1000)

Reagent type (species) or resource	Designation	Source or reference	Identifiers	Additional information
Antibody	HRP-conjugated Beta Actin (Mouse monoclonal)	Proteintech	Cat#: HRP-60008 RRID: AB_2289225	WB (1:10,000)
Commercial assay or kit	Alanine Aminotransaminase (ALT) kit	Sekisui Diagnostics	318-30	
Commercial assay or kit	Aspartate Aminotransferase (AST) kit	Sekisui Diagnostics	319-30	
Commercial assay or kit	Liver Triglyceride	Wako	994-02891	
Commercial assay or kit	Microsome Isolation	Abcam	ab206995	
Commercial assay or kit	NE-PER Nuclear and Cytoplasmic Extraction Reagents	Thermo Fisher Scientific	78833	
Commercial assay or kit	Supersignal West Pico Plus substrate	Thermo Fisher Scientific	34577	
Chemical compound, drug	Ammonium formate	Honeywell	Cat# 55674	
Chemical compound, drug	Methanol	Honeywell	Cat# LC230-4	
Chemical compound, drug	Water	Honeywell	Cat# LC365-4	
Chemical compound, drug	Acetonitrile	Honeywell	Cat# LC015-4	
Chemical compound, drug	Isopropanol	Fisher Scientific	Cat# A461-4	
Chemical compound, drug	Ethyl acetate	Sigma-Aldrich	Cat# 650528	
Chemical compound, drug	Formic acid	Thermo Scientific	Cat# 28905	
Chemical compound, drug	FA 18:0 _{d35}	Cayman Chemical	Cat# 9003318	
Chemical compound, drug	ACar 18:1 _{d3}	Cayman Chemical	Cat# 26578	
Chemical compound, drug	BMP 14:0_14:0	Avanti	Cat# 857131	
Chemical compound, drug	PG 15:0_18:1 _{d7}	Avanti	Cat# 91640	
Chemical compound, drug	Cer d18:1 _{d7_15:0}	Avanti	Cat# 860681P	
Chemical compound, drug	PA 15:0_18:1 _{d7}	Avanti	Cat# 791642	
Chemical compound, drug	SPLASH LipidoMix II	Avanti	Cat# 330709	
Chemical compound, drug	BMP 18:1_18:1	Avanti	Cat# 857133P	
Chemical compound, drug	PG 18:1_18:1	Avanti	Cat# 840475P	

Human studies

Healthy Control and Heavy Drinking Patient Selection – Healthy controls or heavy drinkers with an AUDIT score greater than >16 were recruited from the Clinical Research Unit at the Cleveland Clinic or MetroHealth Hospital in Cleveland, Ohio based on medical history and physical examination. The study protocol was approved by the Institutional Review Board for the Protection of Human Subjects in Research at the Cleveland Clinic (IRB 17-718) and MetroHealth Hospital Cleveland (IRB 18-00911). All methods were performed in accordance with the internal review board's guidelines and regulations, and written, informed consent was obtained from all subjects. Subject demographics are shown in **Figure 1—source data 1**.

Mice and experimental diets

To generate conditional *Mboat7* knockout mice, we obtained 'knockout first' (*Mboat7*^{tm1a(KOMP)Wtsi}) mice from Dr. Philip Hawkins (**Anderson et al., 2013**), and crossed these mice with mice transgenically expressing FLP recombinase to remove the NEO cassette resulting in a conditional *Mboat7* floxed allele. The FLP transgene was then subsequently bred out of the line and resulting *Mboat7*^{fl^{ox}/WT} mice, which were used to expand further downstream tissue-specific knockout lines. To generate congenic hepatocyte-specific (*Mboat7*-HSKO) and myeloid-specific (*Mboat7*-MSKO) *Mboat7* knockout mice we crossed mice harboring a post-FLP recombinase conditionally targeted *Mboat7* floxed allele (**Anderson et al., 2013; Massey et al., 2023**) to mice transgenically expressing Cre recombinase under the albumin promoter/enhancer (**Postic et al., 1999**) or Cre knocked into the M lysozyme locus (**Clausen et al., 1999**), respectively. These independent *Mboat7*-HSKO and *Mboat7*-MSKO lines were then backcrossed mice >10 generations into the C57BL/6J background and subsequently subjected to ethanol exposure. Confirmation of sufficient backcrossing into the C57BL/6J background was confirmed by mouse genome SNP scanning at the Jackson Laboratory (Bar Harbor, ME). Age- and weight-matched female (8–10 weeks old) control (*Mboat7*^{fl^{ox}/fl^{ox}}), hepatocyte-specific *Mboat7* knockout mice (*Mboat7*-HSKO), or myeloid-specific *Mboat7* knockout mice (*Mboat7*-MSKO) were maintained on a chow diet and randomized into pair- and ethanol-fed groups using the NIAAA model (**Bertola et al., 2013**). Briefly, mice were initially fed with control Lieber–DeCarli diet ad libitum for 5 days to acclimatize them to liquid diet. Afterward, ethanol (EtOH)-fed groups were allowed free access to the ethanol Lieber–DeCarli diet containing 5% (vol/vol) ethanol for 10 days, and control groups were pair-fed with the isocaloric substituted maltose dextrins as control diet. At day 11, ethanol- and pair-fed mice were gavaged in the early morning with a single dose of ethanol (5 g/kg body weight) or isocaloric maltose dextrin, respectively, and euthanized 6 hr later (**Bertola et al., 2013**). All mice were maintained in an Association for the Assessment and Accreditation of Laboratory Animal Care, International-approved animal facility, and all experimental protocols were approved by the Institutional Animal Care and Use Committee of the Cleveland Clinic (IACUC protocols # 2018-2053 and # 00002499).

Histological analysis and imaging

Hematoxylin and eosin (H&E) staining of paraffin-embedded liver sections was performed as previously described (**Gromovsky et al., 2017; Warriar et al., 2015; Brown et al., 2010; Brown et al., 2008a; Brown et al., 2008b**). Histopathologic evaluation was scored in a blinded fashion by a board-certified pathologist with expertise in gastrointestinal/liver pathology (Daniela S. Allende – Cleveland Clinic). H&E slides were scanned using a Leica Aperio AT2 Slide Scanner (Leica Microsystems, GmbH, Wetzlar, Germany) and images were processed using ImageScope (Aperio, Software Version 12.1).

Immunoblotting

Whole tissue homogenates were made from tissues in a modified RIPA buffer as previously described (**Warrior et al., 2015; Gwag et al., 2019; Schugar et al., 2017; Lord et al., 2016**), microsome was isolated from the livers of control (*Mboat7*^{fl^{ox}/fl^{ox}}) or hepatocyte-specific *Mboat7* knockout mice (*Mboat7*-HSKO) using microsome isolation kit from Abcam and protein was quantified using the bicinchoninic assay (Pierce). Proteins were separated by 4–12% sodium dodecyl sulfate–polyacrylamide gel electrophoresis transferred to polyvinylidene difluoride membranes, and then proteins were detected after incubation with specific antibodies as previously described (**Warrior et al., 2015; Gwag et al., 2019; Schugar et al., 2017; Lord et al., 2016**) and listed in the Key resources table.

Real-time PCR analysis of gene expression

Tissue RNA extraction and qPCR analysis were performed as previously described (*Gwag et al., 2019*). The mRNA expression levels were calculated based on the $\Delta\Delta CT$ method using cyclophilin A as the housekeeping gene. qPCR was conducted using the Applied Biosystems 7500 Real-Time PCR system. All primer sequences can be found in *Supplementary file 1*.

Plasma and liver biochemistries

To determine the level of hepatic injury in mice fed HFD, plasma was used to analyze ALT levels using enzymatic assays as previously described (*Gwag et al., 2019*). Extraction of liver lipids and quantification of total plasma and hepatic triglycerides were conducted using enzymatic assays as described previously (*Gwag et al., 2019; Gromovsky et al., 2017*).

Liver lipid extraction

Lipids were extracted from liver samples as previously described (*Jain et al., 2022*). Samples were kept on ice throughout the extraction. Briefly, liver was homogenized in 500 μ l of 3:1:6 isopropanol:water:ethyl acetate containing internal standard in ceramic bead tubes (QIAGEN #13113-50) using the TissueLyzer II (QIAGEN #9244420). Samples were centrifuged at 16,000 $\times g$ for 10 min at 4°C and the lipid containing supernatant was transferred to a new 1.5 ml tube. Lipid extracts were dried in a SpeedVac (Thermo Savant RVT5105) and resuspended in 150 μ l of methanol. Samples were kept at 4°C for no more than 1 week before analysis.

Targeted quantification of LPI and PI lipids

Quantitation of LPI and PI species was performed as previously described (*Gwag et al., 2019*). Briefly, LPI and PI standards (LPI 16:0, LPI 18:0, LPI 18:1, LPI 20:4, PI 38:4) and the two internal standards (LPI 17:1-d31, PI 34:1-d31) were purchased Avanti Polar Lipids. High-performance liquid chromatography (HPLC) grade water, methanol, and acetonitrile were purchased from Thermo Fisher Scientific. Standard LPI and PI species at concentrations of 0, 5, 20, 100, 500, and 2000 ng/ml were prepared in 90% methanol containing two internal standards at the concentration of 500 ng/ml. Samples were injected into the Shimadzu LCMS-8050 for generating the internal standard calibration curves. A triple quadrupole mass spectrometer (Quantiva, Thermo Fisher Scientific, Waltham, MA, USA) was used for analysis of LPI and PI species. The mass spectrometer was coupled to the outlet of an UHPLC system (Vanquish, Thermo Fisher Scientific, Waltham, MA, USA), including an auto sampler with refrigerated sample compartment and inline vacuum degasser. The HPLC eluent was directly injected into the triple quadrupole mass spectrometer and the analytes were ionized at ESI (Electrospray Ionization) negative mode. Analytes were quantified using Selected Reaction Monitoring (SRM) and the SRM transitions (m/z) were 571 \rightarrow 255 for LPI 16:0, 599 \rightarrow 283 for LPI 18:0, 597 \rightarrow 281 for LPI 18:1, 619 \rightarrow 303 for LPI 20:4, 885 \rightarrow 241 for PI 38:4, 583 \rightarrow 267 for internal standard LPI 17:1, and 866 \rightarrow 281 for internal standard PI 34:1-d31. Xcalibur software was used to get the peak area for both the internal standards and LPI and PI species. The internal standard calibration curves were used to calculate the concentration of LPI and PI species in the samples.

Untargeted lipidomics

Untargeted lipidomics was performed using an Agilent 1290 Infinity II liquid chromatograph equipped with a Waters Acquity BEH C18 column (1.7 μ m 2.1 \times 100 mm) coupled to an Agilent 6546 Q-TOF mass spectrometer. Mobile phase A was 60:40 acetonitrile:water and B was 90:9:1 isopropanol:acetonitrile:water with both phases buffered with 10 mM ammonium formate and 0.1% formic acid. The gradient was as follows: starting at 15% B to 30% B at 2.40 min, 48% at 3 min, 82% at 13.2 min, 99% at 13.8 min then held at 99% until 15.4 min before equilibrating 15%, held until 20 min. Samples were analyzed in both positive and negative ionizations in separate experiments with the following MS parameters: drying gas flowing 12 l/min at 250°C, nebulizer at 30 psi and sheath gas flowing 11 l/min at 300°C for positive mode. The sheath gas flow was 12 l/min at 375°C with a nebulizer pressure of 30 psi in negative mode. Both ionizations had the same voltage for capillary (4000 V), skimmer (75 V), fragmentor (190 V), and octupole (750 V). Reference masses ($m/z = 121.05$ and 922 for positive mode; 112.98 and 966.00 for negative mode) were continuously infused during sample runs for accurate mass calibration. Pooled samples were run in consecutive iterative MS/MS injections at a constant

collision energy of 25 V to collect spectra for lipid library creation using Agilent LipidAnnotator and MS1 data were collected for all individual samples. Peak integration was performed using Agilent Profinder (v8.0) software and further curation and internal standard normalization were performed using in-house R scripts as described previously (Jain et al., 2022). Untargeted data are reported in units of pmol lipid/g tissue. Principal component analysis and heatmaps were generated using MetaboAnalyst (Pang et al., 2021). The first and second principal components are plotted on the x- and y-axis, respectively, and sample treatment group is indicated by color. For heatmap generation, data were pareto-scaled and the normalized intensity is indicated by color with relative increase in red and decrease in blue. The top 70 lipid features by analysis of variance (ANOVA) p-value are plotted on the y-axis and samples are grouped by Ward clustering on the x-axis. Sample treatments are distinguished by color.

Targeted quantification of BMPs and PGs

Targeted BMP and PG lipid analysis was conducted on an Agilent 1290 Infinity II LC coupled to an Agilent 6495C QQQ mass spectrometer. The same column, mobile phases, and gradient were used for targeted analysis as for the untargeted. The MS parameters for both ionizations were as follows: drying gas temp flow of 12 l/min at 250°C with nebulizer at 35 psi and sheath gas flow of 11 l/min at 300°C. Capillary voltage was kept at 4000 V with nozzle voltage of 500 V and collision energy = 20 V. The iFunnel high pressure RF was at 150/90 V and low-pressure RF at 60/60 V for positive/negative ionizations, respectively. A sample type specific lipid library was created by running pooled liver extract multiple times in positive ionization using multiple reaction monitoring (MRM) to scan for a list of BMP/PG lipid precursor masses ($[\text{NH}_4]^+$ adducts) with transitions for the respective fatty acid and diacylglycerol (-17 m/z) adducts (Grabner et al., 2019). BMPs were identified by the characteristic free fatty acid fragment being much higher intensity than the diacylglycerol fragment, whereas the opposite was true for PG. In addition, BMP lipids eluted between 0.3 and 0.5 min earlier than the isomeric PG counterpart. These distinguishing characteristics were validated using commercial BMP 18:1_18:1 and PG 18:1_18:1 standards. A dynamic MRM method was created using the retention time data gathered from positive ionization tests but in negative mode scanning for the $[\text{M}-\text{H}]^-$ precursors and fatty acid fragments as BMP and PG are much more readily ionized in negative mode. Data were integrated in Agilent Quantitative analysis and peaks were manually adjusted and verified. Final units are in ng lipid/mg tissue.

Lysosome protein degradation activity assay

Lysosome protein degradation activity was performed as previously described (Robinet et al., 2021). Briefly, DQ-ovalbumin (D12053, Thermo Fisher Scientific) was labeled with Alexa Fluor 647 succinimidyl ester (A20006, Thermo Fisher Scientific) at room temperature for 1 hr (3:1 dye:protein mole ratio) to make lysosome protein degradation indicator. The reaction was stopped by incubating the conjugate with 1.5 M hydroxylamine (pH 8.5) for 1 hr at room temperature, and the conjugate was purified by extensive dialysis. Lysosome protein degradation indicator was validated in vitro by incubating with proteinase K and achieving significant increase of Bodipy/Alexa647 ratio (Robinet et al., 2021). The double labeled ovalbumin has increased Bodipy fluorescence upon its degradation by decreasing its self-quenching, while Alexa647 is not changed upon its degradation and is used to normalize for cellular uptake. Wild-type or MBOAT7 Δ -Huh7 hepatoma cells treated with or without 100 mM ethanol for 48 hr were incubated with 10 $\mu\text{g}/\text{ml}$ of lysosome indicator for 2 hr, and lysosome activity was analyzed by flow cytometry in $\approx 10,000$ cells with a LSRFortessa device (BD). Flowjo software was used to export data for each cell for ratiometric analyses, and the median Bodipy/Alexa647 ratio for each independent well was used for analysis.

Statistical analyses

Single comparisons between two groups were performed using two-tailed Student's *t* tests with 95% confidence intervals. Comparisons involving multiple groups beyond binary comparison were assessed using one-way ANOVA with Tukey's post hoc test. All data presented as mean \pm standard error of the mean. Values were considered significant at $p < 0.05$ (using superscripts), or $***p < 0.001$ and $****p < 0.0001$ in Figure 1. JMP 17.0 statistical discovery software (SAS Institute, Cary, NC, USA) was used for all statistical analyses.

Acknowledgements

This work was supported in part by National Institutes of Health grants P50 AA024333 (J.D., S.D., D.S.A., L.E.N., J.M.B.), R01 DK120679 (J.M.B.), RF1 NS133812 (J.M.B.), P01 HL147823 (J.M.B.), U01 AA026938 (L.E.N., J.M.B.), R01 DK130227 (J.M.B.), U01 AA026264 (L.E.N.), R01 HL128268 (J.D.S.), JDRF JDRF201309442 (J.S.), the Glenn and AFAR Junior Faculty Grant A22068 (J.S.), R01 DK133479 (J.S.); Hatch Grant WIS04000 (R.J., J.S.), K01 DK128022 (R.N.H.), UL1TR001998 (R.N.H.), and the American Heart Association-Postdoctoral Fellowships 19POST34380725 (I.R.). The authors would like to thank Dr. Philip Hawkins (Babraham Institute) for providing *Mboat7* knockout first mice.

Additional information

Competing interests

Judith Simcox, J Mark Brown: Reviewing editor, *eLife*. The other authors declare that no competing interests exist.

Funding

Funder	Grant reference number	Author
NIH Office of the Director	P50 AA024333	Srinivasan Dasarathy Daniela S Allende Jonathan D Smith Laura E Nagy J Mark Brown
NIH Office of the Director	R01 DK120679	J Mark Brown
NIH Office of the Director	RF1 NS133812	J Mark Brown
NIH Office of the Director	P01 HL147823	J Mark Brown
NIH Office of the Director	U01 AA026938	Laura E Nagy J Mark Brown
NIH Office of the Director	R01 DK130227	J Mark Brown
NIH Office of the Director	U01 AA026264	J Mark Brown
NIH Office of the Director	R01 HL128268	Jonathan D Smith
JDRF	JDRF201309442	Judith Simcox
Glenn Foundation for Medical Research	A22068	Judith Simcox
NIH Office of the Director	R01 DK133479	Judith Simcox
University of Wisconsin-Madison	WIS04000	Raghav Jain Judith Simcox
NIH Office of the Director	DK128022	Robert N Helsley
University of Kentucky	UL1TR001998	Robert N Helsley
American Heart Association	19POST34380725	Iyappan Ramachandiran

The funders had no role in study design, data collection, and interpretation, or the decision to submit the work for publication.

Author contributions

Venkateshwari Varadharajan, Conceptualization, Resources, Data curation, Software, Formal analysis, Validation, Investigation, Visualization, Methodology, Writing – original draft, Writing – review and editing; Iyappan Ramachandiran, Rakhee Banerjee, Anthony J Horak, Megan R McMullen, Annette Bellar, Shuhui W Lorkowski, Kailash Gulshan, Isabella James, Nicole Welch, Data curation, Formal analysis, Validation, Investigation, Visualization, Methodology, Writing – review and editing; William J Massey, Data curation, Investigation, Visualization, Methodology, Writing – review and editing; Raghav

Jain, Data curation, Formal analysis, Investigation, Visualization, Methodology, Writing – review and editing; Emily Huang, Data curation, Validation, Investigation, Visualization, Methodology, Writing – review and editing; Robert N Helsley, Vai Pathak, Data curation, Formal analysis, Validation, Investigation, Visualization, Methodology; Jaividhya Dasarathy, Srinivasan Dasarathy, David Stroom, Ofer Reizes, Daniela S Allende, Jonathan D Smith, Judith Simcox, Data curation, Formal analysis, Supervision, Validation, Investigation, Visualization, Methodology, Writing – review and editing; Laura E Nagy, Data curation, Formal analysis, Supervision, Validation, Investigation, Visualization, Methodology, Writing – review and editing, helped design experiments and provided useful discussion directing collaborative aspects of the project; J Mark Brown, Conceptualization, Resources, Data curation, Software, Formal analysis, Supervision, Funding acquisition, Validation, Investigation, Visualization, Methodology, Writing – original draft, Project administration, Writing – review and editing

Author ORCIDs

Venkateshwari Varadharajan  <http://orcid.org/0000-0002-4557-9840>

William J Massey  <https://orcid.org/0000-0002-2087-6048>

Raghav Jain  <http://orcid.org/0000-0002-1284-6762>

Robert N Helsley  <http://orcid.org/0000-0001-5000-3187>

Isabella James  <https://orcid.org/0009-0000-2796-3497>

Srinivasan Dasarathy  <http://orcid.org/0000-0003-1774-0104>

Jonathan D Smith  <http://orcid.org/0000-0002-0415-386X>

Judith Simcox  <http://orcid.org/0000-0001-7350-6342>

J Mark Brown  <https://orcid.org/0000-0003-2708-7487>

Ethics

The study protocol was approved by the Institutional Review Board for the Protection of Human Subjects in Research at the Cleveland Clinic (IRB 17-718) and MetroHealth Hospital Cleveland (IRB 18-00911). All methods were performed in accordance with the internal review board's guidelines and regulations, and written, informed consent was obtained from all subjects.

All mice were maintained in an Association for the Assessment and Accreditation of Laboratory Animal Care, International-approved animal facility, and all experimental protocols were approved by the Institutional Animal Care and Use Committee of the Cleveland Clinic (IACUC protocols # 2018-2053 and # 00002499).

Peer review material

Reviewer #2 (Public Review): <https://doi.org/10.7554/eLife.92243.3.sa1>

Author response <https://doi.org/10.7554/eLife.92243.3.sa2>

Additional files

Supplementary files

- Supplementary file 1. Primers.
- MDAR checklist

Data availability

All data generated or analyzed during this study are included in the manuscript and supporting files.

References

- Alharthi J**, Bayoumi A, Thabet K, Pan Z, Gloss BS, Latchoumanin O, Lundberg M, Twine NA, McLeod D, Alenizi S, Adams LA, Weltman M, Berg T, Liddle C, George J, Eslam M. 2022. A metabolic associated fatty liver disease risk variant in MBOAT7 regulates toll like receptor induced outcomes. *Nature Communications* **13**:7430. DOI: <https://doi.org/10.1038/s41467-022-35158-9>, PMID: 36473860
- Anderson KE**, Kielkowska A, Durrant TN, Juvin V, Clark J, Stephens LR, Hawkins PT. 2013. Lysophosphatidylinositol-acyltransferase-1 (LPIAT1) is required to maintain physiological levels of PtdIns and PtdInsP(2) in the mouse. *PLOS ONE* **8**:e58425. DOI: <https://doi.org/10.1371/journal.pone.0058425>, PMID: 23472195
- Baba T**, Balla T. 2020. Emerging roles of phosphatidylinositol 4-phosphate and phosphatidylinositol 4,5-bisphosphate as regulators of multiple steps in autophagy. *Journal of Biochemistry* **168**:329–336. DOI: <https://doi.org/10.1093/jb/mvaa089>, PMID: 32745205

- Bala S**, Szabo G. 2018. TFEB, a master regulator of lysosome biogenesis and autophagy, is a new player in alcoholic liver disease. *Digestive Medicine Research* **1**:16. DOI: <https://doi.org/10.21037/dmr.2018.09.03>, PMID: 30450489
- Beaudoin JJ**, Liang T, Tang Q, Banini BA, Shah VH, Sanyal AJ, Chalasani NP, Gawrieh S. 2021. Role of candidate gene variants in modulating the risk and severity of alcoholic hepatitis. *Alcoholism, Clinical and Experimental Research* **45**:709–719. DOI: <https://doi.org/10.1111/acer.14581>, PMID: 33616244
- Bertola A**, Mathews S, Ki SH, Wang H, Gao B. 2013. Mouse model of chronic and binge ethanol feeding (the NIAAA model). *Nature Protocols* **8**:627–637. DOI: <https://doi.org/10.1038/nprot.2013.032>, PMID: 23449255
- Brown JM**, Chung S, Sawyer JK, Degirolamo C, Alger HM, Nguyen T, Zhu X, Duong MN, Wibley AL, Shah R, Davis MA, Kelley K, Wilson MD, Kent C, Parks JS, Rudel LL. 2008a. Inhibition of stearyl-coenzyme A desaturase 1 dissociates insulin resistance and obesity from atherosclerosis. *Circulation* **118**:1467–1475. DOI: <https://doi.org/10.1161/CIRCULATIONAHA.108.793182>, PMID: 18794388
- Brown JM**, Bell TA, Alger HM, Sawyer JK, Smith TL, Kelley K, Shah R, Wilson MD, Davis MA, Lee RG, Graham MJ, Crooke RM, Rudel LL. 2008b. Targeted depletion of hepatic ACAT2-driven cholesterol esterification reveals a non-biliary route for fecal neutral sterol loss. *The Journal of Biological Chemistry* **283**:10522–10534. DOI: <https://doi.org/10.1074/jbc.M707659200>, PMID: 18281279
- Brown JM**, Betters JL, Lord C, Ma Y, Han X, Yang K, Alger HM, Melchior J, Sawyer J, Shah R, Wilson MD, Liu X, Graham MJ, Lee R, Crooke R, Shulman GI, Xue B, Shi H, Yu L. 2010. CGI-58 knockdown in mice causes hepatic steatosis but prevents diet-induced obesity and glucose intolerance. *Journal of Lipid Research* **51**:3306–3315. DOI: <https://doi.org/10.1194/jlr.M010256>, PMID: 20802159
- Buch S**, Stickel F, Trépo E, Way M, Herrmann A, Nischalke HD, Brosch M, Rosendahl J, Berg T, Ridinger M, Rietschel M, McQuillin A, Frank J, Kiefer F, Schreiber S, Lieb W, Soyka M, Semmo N, Aigner E, Datz C, et al. 2015. A genome-wide association study confirms PNPLA3 and identifies TM6SF2 and MBOAT7 as risk loci for alcohol-related cirrhosis. *Nature Genetics* **47**:1443–1448. DOI: <https://doi.org/10.1038/ng.3417>, PMID: 26482880
- Chao X**, Wang S, Zhao K, Li Y, Williams JA, Li T, Chavan H, Krishnamurthy P, He XC, Li L, Ballabio A, Ni HM, Ding WX. 2018. Impaired tfeb-mediated lysosome biogenesis and autophagy promote chronic ethanol-induced liver injury and steatosis in mice. *Gastroenterology* **155**:865–879. DOI: <https://doi.org/10.1053/j.gastro.2018.05.027>, PMID: 29782848
- Clark J**, Anderson KE, Juvin V, Smith TS, Karpe F, Wakelam MJO, Stephens LR, Hawkins PT. 2011. Quantification of PtdInsP3 molecular species in cells and tissues by mass spectrometry. *Nature Methods* **8**:267–272. DOI: <https://doi.org/10.1038/nmeth.1564>, PMID: 21278744
- Clausen BE**, Burkhardt C, Reith W, Renkawitz R, Förster I. 1999. Conditional gene targeting in macrophages and granulocytes using LysMcre mice. *Transgenic Research* **8**:265–277. DOI: <https://doi.org/10.1023/a:1008942828960>, PMID: 10621974
- Cohen JC**, Horton JD, Hobbs HH. 2011. Human fatty liver disease: old questions and new insights. *Science* **332**:1519–1523. DOI: <https://doi.org/10.1126/science.1204265>, PMID: 21700865
- Fleming MF**, Barry KL, MacDonald R. 1991. The alcohol use disorders identification test (AUDIT) in a college sample. *The International Journal of the Addictions* **26**:1173–1185. DOI: <https://doi.org/10.3109/10826089109062153>, PMID: 1743817
- Fruman DA**, Chiu H, Hopkins BD, Bagrodia S, Cantley LC, Abraham RT. 2017. The pi3k pathway in human disease. *Cell* **170**:605–635. DOI: <https://doi.org/10.1016/j.cell.2017.07.029>, PMID: 28802037
- Gijón MA**, Riekhof WR, Zarini S, Murphy RC, Voelker DR. 2008. Lysophospholipid acyltransferases and arachidonate recycling in human neutrophils. *The Journal of Biological Chemistry* **283**:30235–30245. DOI: <https://doi.org/10.1074/jbc.M806194200>, PMID: 18772128
- Grabner GF**, Fawzy N, Pribasniq MA, Trieb M, Taschler U, Holzer M, Schweiger M, Wolinski H, Kolb D, Horvath A, Breinbauer R, Rüllicke T, Rabl R, Lass A, Stadlbauer V, Hutter-Paier B, Stauber RE, Fickert P, Zechner R, Marsche G, et al. 2019. Metabolic disease and ABHD6 alter the circulating bis(monoacylglycerol) phosphate profile in mice and humans. *Journal of Lipid Research* **60**:1020–1031. DOI: <https://doi.org/10.1194/jlr.M093351>, PMID: 30894461
- Gromovsky AD**, Schugar RC, Brown AL, Helsley RN, Burrows AC, Ferguson D, Zhang R, Sansbury BE, Lee RG, Morton RE, Allende DS, Parks JS, Spite M, Brown JM. 2017. Δ-5 fatty acid desaturase fads1 impacts metabolic disease by balancing proinflammatory and proresolving lipid mediators. *Arteriosclerosis, Thrombosis, and Vascular Biology* **38**:218–231. DOI: <https://doi.org/10.1161/ATVBAHA.117.309660>
- Gruenberg J**. 2020. Life in the lumen: the multivesicular endosome. *Traffic* **21**:76–93. DOI: <https://doi.org/10.1111/tra.12715>, PMID: 31854087
- Gwag T**, Meng Z, Sui Y, Helsley RN, Park SH, Wang S, Greenberg RN, Zhou C. 2019. Non-nucleoside reverse transcriptase inhibitor efavirenz activates PXR to induce hypercholesterolemia and hepatic steatosis. *Journal of Hepatology* **70**:930–940. DOI: <https://doi.org/10.1016/j.jhep.2018.12.038>, PMID: 30677459
- Hoxhaj G**, Manning BD. 2020. The PI3K-AKT network at the interface of oncogenic signalling and cancer metabolism. *Nature Reviews. Cancer* **20**:74–88. DOI: <https://doi.org/10.1038/s41568-019-0216-7>, PMID: 31686003
- Hullin-Matsuda F**, Taguchi T, Greimel P, Kobayashi T. 2014. Lipid compartmentalization in the endosome system. *Seminars in Cell & Developmental Biology* **31**:48–56. DOI: <https://doi.org/10.1016/j.semcdb.2014.04.010>, PMID: 24747366

- Jain R, Wade G, Ong I, Chaurasia B, Simcox J. 2022. Determination of tissue contributions to the circulating lipid pool in cold exposure via systematic assessment of lipid profiles. *Journal of Lipid Research* **63**:100197. DOI: <https://doi.org/10.1016/j.jlr.2022.100197>, PMID: 35300982
- Krawczyk M, Rau M, Schattenberg JM, Bantel H, Pathil A, Demir M, Kluge J, Boettler T, Lammert F, Geier A, NAFLD Clinical Study Group. 2017. Combined effects of the PNPLA3 rs738409, TM6SF2 rs58542926, and MBOAT7 rs641738 variants on NAFLD severity: a multicenter biopsy-based study. *Journal of Lipid Research* **58**:247–255. DOI: <https://doi.org/10.1194/jlr.P067454>, PMID: 27836992
- Lord CC, Ferguson D, Thomas G, Brown AL, Schugar RC, Burrows A, Gromovsky AD, Betters J, Neumann C, Sacks J, Marshall S, Watts R, Schweiger M, Lee RG, Crooke RM, Graham MJ, Lathia JD, Sakaguchi TF, Lehner R, Haemmerle G, et al. 2016. Regulation of Hepatic Triacylglycerol Metabolism by CGI-58 Does Not Require ATGL Co-activation. *Cell Reports* **16**:939–949. DOI: <https://doi.org/10.1016/j.celrep.2016.06.049>, PMID: 27396333
- Mancina RM, Dongiovanni P, Petta S, Pingitore P, Meroni M, Rametta R, Borén J, Montalcini T, Pujia A, Wiklund O, Hindy G, Spagnuolo R, Motta BM, Pipitone RM, Craxì A, Fargion S, Nobili V, Käkelä P, Kärjä V, Männistö V, et al. 2016. The mboat7-tmc4 variant rs641738 increases risk of nonalcoholic fatty liver disease in individuals of european descent. *Gastroenterology* **150**:1219–1230. DOI: <https://doi.org/10.1053/j.gastro.2016.01.032>, PMID: 26850495
- Massey WJ, Varadharajan V, Banerjee R, Brown AL, Horak AJ, Hohe RC, Jung BM, Qiu Y, Chan ER, Pan C, Zhang R, Allende DS, Willard B, Cheng F, Lusis AJ, Brown JM. 2023. MBOAT7-driven lysophosphatidylinositol acylation in adipocytes contributes to systemic glucose homeostasis. *Journal of Lipid Research* **64**:100349. DOI: <https://doi.org/10.1016/j.jlr.2023.100349>, PMID: 36806709
- Meroni M, Dongiovanni P, Longo M, Carli F, Baselli G, Rametta R, Pelusi S, Badiali S, Maggioni M, Gaggini M, Fracanzani AL, Romeo S, Gatti S, Davidson NO, Gastaldelli A, Valenti L. 2020. Mboat7 down-regulation by hyper-insulinemia induces fat accumulation in hepatocytes. *EBioMedicine* **52**:102658. DOI: <https://doi.org/10.1016/j.ebiom.2020.102658>, PMID: 32058943
- Pang Z, Chong J, Zhou G, de Lima Morais DA, Chang L, Barrette M, Gauthier C, Jacques PÉ, Li S, Xia J. 2021. MetaboAnalyst 5.0: narrowing the gap between raw spectra and functional insights. *Nucleic Acids Research* **49**:W388–W396. DOI: <https://doi.org/10.1093/nar/gkab382>, PMID: 34019663
- Pemberton JG, Kim YJ, Balla T. 2020. Integrated regulation of the phosphatidylinositol cycle and phosphoinositide-driven lipid transport at ER-PM contact sites. *Traffic* **21**:200–219. DOI: <https://doi.org/10.1111/tra.12709>, PMID: 31650663
- Postic C, Shiota M, Niswender KD, Jetton TL, Chen Y, Moates JM, Shelton KD, Lindner J, Cherrington AD, Magnuson MA. 1999. Dual roles for glucokinase in glucose homeostasis as determined by liver and pancreatic beta cell-specific gene knock-outs using Cre recombinase. *The Journal of Biological Chemistry* **274**:305–315. DOI: <https://doi.org/10.1074/jbc.274.1.305>, PMID: 9867845
- Rinella ME, Sanyal AJ. 2016. Management of NAFLD: a stage-based approach. *Nature Reviews. Gastroenterology & Hepatology* **13**:196–205. DOI: <https://doi.org/10.1038/nrgastro.2016.3>, PMID: 26907882
- Robinet P, Ritchey B, Lorkowski SW, Alzayed AM, DeGeorgia S, Schodowski E, Traughber CA, Smith JD. 2021. Quantitative trait locus mapping identifies the Gpnmb gene as a modifier of mouse macrophage lysosome function. *Scientific Reports* **11**:10249. DOI: <https://doi.org/10.1038/s41598-021-89800-5>, PMID: 33986446
- Rouzer CA, Ivanova PT, Byrne MO, Brown HA, Marnett LJ. 2007. Lipid profiling reveals glycerophospholipid remodeling in zymosan-stimulated macrophages. *Biochemistry* **46**:6026–6042. DOI: <https://doi.org/10.1021/bi0621617>, PMID: 17458939
- Sabatine MS. 2019. PCSK9 inhibitors: clinical evidence and implementation. *Nature Reviews. Cardiology* **16**:155–165. DOI: <https://doi.org/10.1038/s41569-018-0107-8>, PMID: 30420622
- Schink KO, Tan KW, Stenmark H. 2016. Phosphoinositides in control of membrane dynamics. *Annual Review of Cell and Developmental Biology* **32**:143–171. DOI: <https://doi.org/10.1146/annurev-cellbio-111315-125349>, PMID: 27576122
- Schugar RC, Shih DM, Warriar M, Helsley RN, Burrows A, Ferguson D, Brown AL, Gromovsky AD, Heine M, Chatterjee A, Li L, Li XS, Wang Z, Willard B, Meng Y, Kim H, Che N, Pan C, Lee RG, Crooke RM, et al. 2017. The tmao-producing enzyme flavin-containing monooxygenase 3 regulates obesity and the beiging of white adipose tissue. *Cell Reports* **19**:2451–2461. DOI: <https://doi.org/10.1016/j.celrep.2017.05.077>, PMID: 28636934
- Shindou H, Shimizu T. 2009. Acyl-CoA:lysophospholipid acyltransferases. *The Journal of Biological Chemistry* **284**:1–5. DOI: <https://doi.org/10.1074/jbc.R800046200>, PMID: 18718904
- Showalter MR, Berg AL, Nagourney A, Heil H, Carraway KL, Fiehn O. 2020. The emerging and diverse roles of bis(monoacylglycero) phosphate lipids in cellular physiology and disease. *International Journal of Molecular Sciences* **21**:8067. DOI: <https://doi.org/10.3390/ijms21218067>, PMID: 33137979
- Stickel F, Buch S, Nischalke HD, Weiss KH, Gotthardt D, Fischer J, Rosendahl J, Marot A, Elamy M, Casper M, Lammert F, McQuillin A, Zopf S, Spengler U, Marhenke S, Kirstein MM, Vogel A, Eyer F, von Felden J, Wege H, et al. 2018. Genetic variants in PNPLA3 and TM6SF2 predispose to the development of hepatocellular carcinoma in individuals with alcohol-related cirrhosis. *The American Journal of Gastroenterology* **113**:1475–1483. DOI: <https://doi.org/10.1038/s41395-018-0041-8>, PMID: 29535416
- Tanaka Y, Shimanaka Y, Caddeo A, Kubo T, Mao Y, Kubota T, Kubota N, Yamauchi T, Mancina RM, Baselli G, Luukkonen P, Pihlajamäki J, Yki-Järvinen H, Valenti L, Arai H, Romeo S, Kono N. 2021. LPIAT1/MBOAT7 depletion increases triglyceride synthesis fueled by high phosphatidylinositol turnover. *Gut* **70**:180–193. DOI: <https://doi.org/10.1136/gutjnl-2020-320646>, PMID: 32253259

- Teo K**, Abeysekera KWM, Adams L, Aigner E, Anstee QM, Banales JM, Banerjee R, Basu P, Berg T, Bhatnagar P, Buch S, Canbay A, Caprio S, Chatterjee A, Ida Chen JD, Chowdhury A, Daly AK, Datz C, Gracia Hahn D, DiStefano JK. 2021. rs641738C>T near MBOAT7 is associated with liver fat, ALT and fibrosis in NAFLD: A meta-analysis. *J. Hepatol* **74**:20–30. DOI: <https://doi.org/10.1016/j.jhep.2020.08.027>
- Thabet K**, Asimakopoulos A, Shojaei M, Romero-Gomez M, Mangia A, Irving WL, Berg T, Dore GJ, Grønbaek H, Sheridan D, Abate ML, Bugianesi E, Weltman M, Mollison L, Cheng W, Riordan S, Fischer J, Spengler U, Nattermann J, Wahid A, et al. 2016. MBOAT7 rs641738 increases risk of liver inflammation and transition to fibrosis in chronic hepatitis C. *Nature Communications* **7**:12757. DOI: <https://doi.org/10.1038/ncomms12757>, PMID: 27630043
- Thabet K**, Chan HLY, Petta S, Mangia A, Berg T, Boonstra A, Brouwer WP, Abate ML, Wong VWS, Nazmy M, Fischer J, Liddle C, George J, Eslam M. 2017. The membrane-bound O-acyltransferase domain-containing 7 variant rs641738 increases inflammation and fibrosis in chronic hepatitis B. *Hepatology* **65**:1840–1850. DOI: <https://doi.org/10.1002/hep.29064>, PMID: 28109005
- Thangapandi VR**, Knittelfelder O, Brosch M, Patsenker E, Vvedenskaya O, Buch S, Hinz S, Hendricks A, Nati M, Herrmann A, Rekhade DR, Berg T, Matz-Soja M, Huse K, Klipp E, Pauling JK, Wodke JA, Miranda Ackerman J, von Bonin M, Aigner E, et al. 2021. Loss of hepatic Mboat7 leads to liver fibrosis. *Gut* **70**:940–950. DOI: <https://doi.org/10.1136/gutjnl-2020-320853>, PMID: 32591434
- Warrier M**, Shih DM, Burrows AC, Ferguson D, Gromovsky AD, Brown AL, Marshall S, McDaniel A, Schugar RC, Wang Z, Sacks J, Rong X, de Vallim TA, Chou J, Ivanova PT, Myers DS, Brown HA, Lee RG, Croke RM, Graham MJ, et al. 2015. The tmao-generating enzyme flavin monooxygenase 3 is a central regulator of cholesterol balance. *Cell Reports* **10**:326–338. DOI: <https://doi.org/10.1016/j.celrep.2014.12.036>, PMID: 25600868
- Wymann MP**, Schneider R. 2008. Lipid signalling in disease. *Nature Reviews. Molecular Cell Biology* **9**:162–176. DOI: <https://doi.org/10.1038/nrm2335>, PMID: 18216772
- Xia M**, Chandrasekaran P, Rong S, Fu X, Mitsche MA. 2021. Hepatic deletion of Mboat7 (LPIAT1) causes activation of SREBP-1c and fatty liver. *Journal of Lipid Research* **62**:100031. DOI: <https://doi.org/10.1194/jlr.RA120000856>, PMID: 32859645
- Zarini S**, Hankin JA, Murphy RC, Gijón MA. 2014. Lysophospholipid acyltransferases and arachidonate recycling in human neutrophils. *Prostaglandins & Other Lipid Mediators* **113–115**:52–61. DOI: <https://doi.org/10.1016/j.prostaglandins.2014.08.003>
- Zhang Y**, Guo T, Yang F, Mao Y, Li L, Liu C, Sun Q, Li Y, Huang J. 2018. Single-nucleotide rs738409 polymorphisms in the PNPLA3 gene are strongly associated with alcoholic liver disease in Han Chinese males. *Hepatology International* **12**:429–437. DOI: <https://doi.org/10.1007/s12072-018-9889-3>, PMID: 30132178